

Simulation of a Sensor Array for Multi-Parameter Measurements at the Prosthetic Limb Interface

Gabriel I. Rowe* and Alexander V. Mamishev

Department of Electrical Engineering, University of Washington, Seattle, WA, USA

ABSTRACT

Sensitive skin is a highly desired device for biomechanical devices, wearable computing, human-computer interfaces, exoskeletons, and, most pertinent to this paper, for lower limb prosthetics. The measurement of shear stress is very important because shear effects are key factors in developing surface abrasions and pressure sores in paraplegics and users of prosthetic/orthotic devices. A single element of a sensitive skin is simulated and characterized in this paper. Conventional tactile sensors are designed for measurement of the normal stress only, which is inadequate for comprehensive assessment of surface contact conditions. The sensitive skin discussed here is a flexible array capable of sensing shear and normal forces, as well as humidity and temperature on each element.

Keywords: Sensitive skin, sensors, prosthetic devices.

1. INTRODUCTION

The goal of sensitive skin is to create an electronic analog to human skin, and improve on it for multi-sensor information gathering. The generic definition of sensitive skin is an array of sensors constructed on a flexible substrate. Such a device often contains multiple types of sensors, or can sense multiple phenomena with one sensor. Sensitive skin devices have increased in complexity since their introduction, e.g. a robotic arm collision avoidance method^{1,2,3}. The abilities and construction of the sensitive skin have varied widely. For instance, using complimentary light emitting diode and photo detector pairs, a sensitive skin was developed for proximity sensing⁴. The sensor introduced by Chase and Luo uses ratios of capacitance on parallel plate capacitive sensors to determine shear and normal forces for robotic grip sensing with a single sensor⁵, and is similar to the method presented in this paper. The ability to determine shear or normal forces separately and at high resolution has been demonstrated using tactile sensing arrays^{6,7}. However, measurement of both forces at the same time in a flexible sensitive skin array has not yet been achieved. While it was anticipated as early as 1998⁷, a flexible normal and shear force device has remained elusive. Although several attempts have been made to manufacture sensor arrays capable of simultaneous measurement of both normal and shear forces, those with adequate field performance and reliability are not flexible^{8,9,10,11} or are macro-scale single element devices⁵. The preliminary modeling of a flexible normal and shear force sensitive skin is discussed here. With normal and shear force sensors as well as the addition of temperature and humidity sensors, the sensitive skin presented here allows measurement of several physical variables using one sensing principle.

The primary motivation for the sensitive skin design in this paper is for its employment as a distributed pressure-sensing device between a lower limb prosthetic device and the residual limb. This work is similar to the analysis done on a distributed pressure sensing array for plantar pressures¹². Determination of shear and normal forces at the interface between a residual lower limb and a prosthetic device is important for prevention of pain and ultimately pressure sores. The humidity and temperature sensing elements are also included for analysis of the conditions associated with particular pressure events. For example, a relation between humidity levels and the likelihood of shear force events could be determined. Previous work has motivated the desire to have pressure measurements integrated into a real-time pressure dissipation system in prosthetic devices¹³. For example, if the pressure exceeds a certain threshold, an actuator relieves the pressure in a localized fashion. The high-impact location for the application of the sensitive skin proposed dictates the need for a sensing technique capable of performing in non-ideal conditions.

Both authors are with SEAL (Sensors, Energy, and Automation Laboratory), Department of Electrical Engineering, Box 352500, University of Washington, Seattle, WA 98195. (E-mail: *gaber@ee.washington.edu; mamishev@ee.washington.edu)

2. SENSOR DESIGN

The sensor is designed so that only capacitive measurements are needed. This increases the robustness of the sensor to maintain performance in the proposed application environment as well as simplifies fabrication and circuit design. The single element sensor modeled in this paper integrates three distinct sensing functions: temperature, humidity and spatial localization. The top layer includes the driving electrodes, temperature sensing electrodes, and humidity sensing electrodes as shown in Fig. 1. Temperature and humidity sensitive functional material are placed on this top layer and are exposed to the environment. The temperature and humidity sensors are coplanar with the driving electrode and employ fringing electric fields that pass through the functional material in order to sense a change in the dielectric permittivity. There is a known relationship between temperature or humidity and the dielectric material of choice. Selected functional materials are evaluated for future implementation. The final selection of materials will rely heavily on the chosen microfabrication technique.

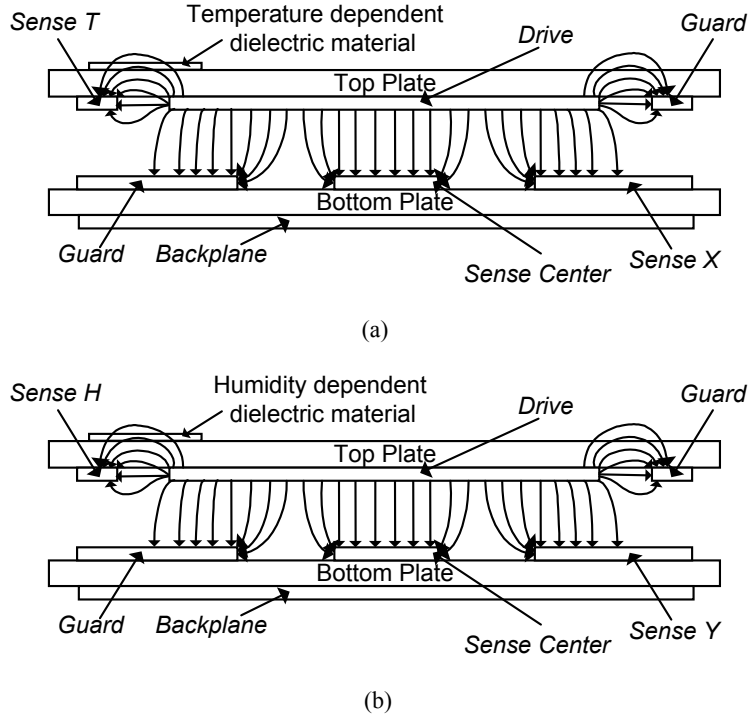


Fig. 1. Cutaway views of the sensor to show electric field lines between electrodes. The temperature and humidity capacitive sensors are shown in a fringing electric field configuration on the left in (a) and (b) respectively. Whereas, the electrodes for determining spatial location are in a parallel plate configuration. (a) depicts the *Sense X* and *Sense C* electrodes, whereas (b) depicts the *Sense Y* and *Sense C* electrodes.

Guard electrodes are used on this layer to limit fringing electric field effects on the sensing electrodes located on the bottom layer. The middle layer is a non-conductive dielectric material. The bottom layer has a center and two side electrodes. The three capacitance values are measured between these electrodes and the *Drive* electrode. The use of the guard electrodes enables simplification of the capacitance calculations to approach the simple two parallel plate condition which are sufficiently close to each other (1). The capacitance is calculated between the driving electrode and the five sensing electrodes: *Sense C*, *Sense X*, *Sense Y*, *Sense H*, and *Sense T*. By changing the geometry of the capacitors, the capacitance value can be used to find the relative displacements between the electrodes.

$$C = \frac{\epsilon_r \epsilon_0 A}{d} \quad (1)$$

The middle layer of the sensor allows a known degree of normal force compressibility and lateral shear movement. A single cell of the sensitive skin array is shown in Fig. 1 and depicts the top and bottom layers with generalized field

lines. The sensor can be visualized more easily by looking at the configuration of the top and bottom planes. Fig. 1 also shows the temperature and humidity dependant materials and the field lines associated with this part of the sensor. The temperature and humidity sensitive materials are omitted from Fig. 2 for simplicity, but would be placed above the *Sense T* and *Sense H* electrodes. The bottom plate also has a grounded backplane, which spans the entire sensitive skin array. Fig. 3 shows the 3D model and a surface plot of electric field magnitudes.

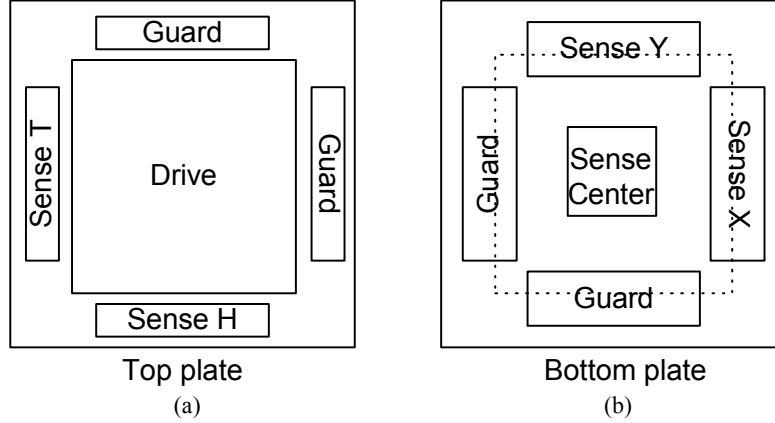


Fig. 2. Top (a) and bottom (b) plate configurations. The top plate lies centered directly over the bottom layer in the zero displacement position such that each sensing electrode, except the center electrode, is opposed by a guard electrode.

3. SENSING METHODOLOGY

The sensor only uses capacitances to transduce position, humidity and temperature. Three electrodes were chosen to determine relative displacements between plates. The center electrode, S_C , was chosen to be central and small to exhibit a small change in capacitance as the large drive plate above it moved laterally. The S_X and S_Y electrodes were chosen to be symmetric and perpendicular in order to sense motion in the X and Y directions. The capacitances between the *Drive* electrode and the sensing electrodes (C_C , C_X , C_Y) are affected by three factors: (i) the overlap of the *Drive* electrode above a sensing electrode; (ii) the electrode/plate separation; (iii) the distance between the edges of the electrodes without overlap of the *Drive* and sense electrodes. Factor (i) has a strong correlation with area, A , whereas factor (ii) is strongly related to electrode/plate separation, d . Finally, factor (iii) is in the region of fringing electric fields and affects both A and d . The capacitance between the *Drive* and sensing electrodes is determined by measuring the voltage on the sensing electrode and calculating the gain of the sinusoidal signal on the *Drive* electrode.

4. SIMULATION METHOD

The sensor was designed and simulated to determine a sensor configuration that functioned as desired using electrostatic finite element analysis software, Ansoft Maxwell 3D Field Simulator. The model simulated is shown with the plates centered over each other in Fig. 3. The sensor cell size modeled is 4 by 4 mm. The *Drive* electrode is 2.6 by 2.6 mm and is surrounded by four symmetrically placed rectangular electrodes with the dimensions of 0.3 by 2.0 mm, see Fig. 2a. The *Center* electrode, S_C , is 0.8 by 0.8 mm. Also surrounding the S_C electrode are four symmetrically placed rectangular electrodes measuring 0.7 by 2.0 mm.

A single element model was simulated to calculate the capacitance values between *Drive* and sensing electrode S_C , S_X , S_Y , S_H , and S_T . The capacitance on each sensing electrode is termed C_C , C_X , C_Y , C_H , and C_T respectively. Custom macros and scripts automated the process of placing the plates in a new location and simulating the model. Each position produced a capacitance matrix with a capacitance value between each object in the model. The capacitance values of interest were extracted and analyzed in Matlab. The simulation resulted in capacitance values ranging from 11 fF up to 277 fF for C_X and C_Y . As expected, C_C remained essentially constant for a constant plate separation.

The simulated plate displacements were performed along cylindrical coordinate axes instead of Cartesian coordinates. Since the plates are connected by a compressible material in the prototype, it is assumed that displacements along radii from a common center point best simulate the manner in which the two plates should move relative to each other. For the simplification of this model, the plates were also assumed to maintain a parallel orientation at all times.

The plate displacements were then converted to Cartesian coordinates in order to simplify the capacitance and location relationship analysis.

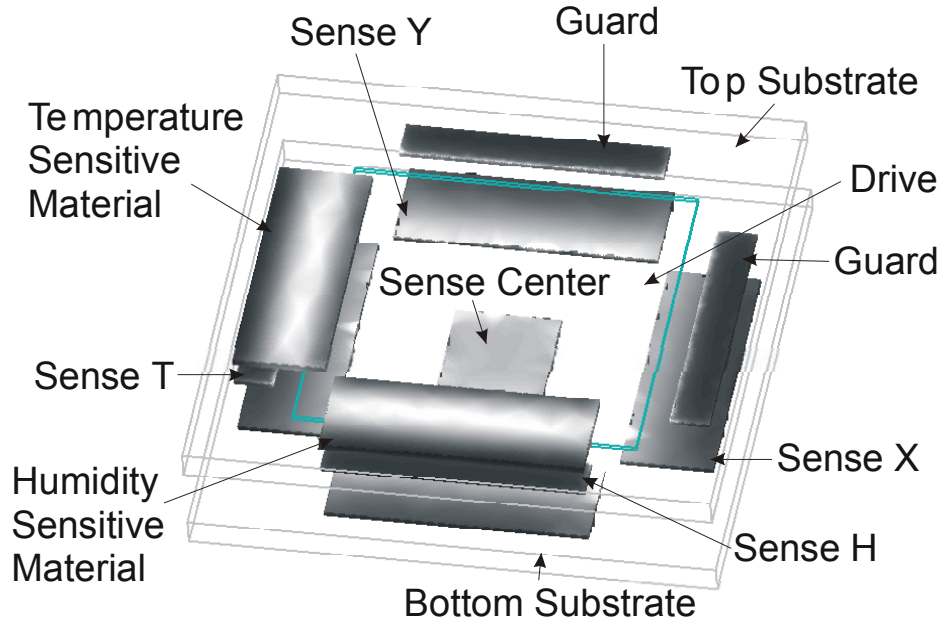


Fig. 3. Sensitive skin single sensor cell simulation of electric field magnitudes on each surface. Lighter shades indicate higher field intensities.

The sensor was analyzed on the axes depicted in Fig. 4. The radial displacement, r , varies from 0 to 420 microns. The azimuthal displacement, θ , varies from 0 to 360 in 22.5° increments. The reference or zero displacement point for θ is when C_Y is a maximum for a constant plate separation. Five plate separations, z , were computed at 450, 350, 250, 150 and 50 micrometer separations. Numbering 565 points in total: 7 radial, 16 azimuthal and 1 center position per plate separation—the data was found to be sufficient for curve fitting.

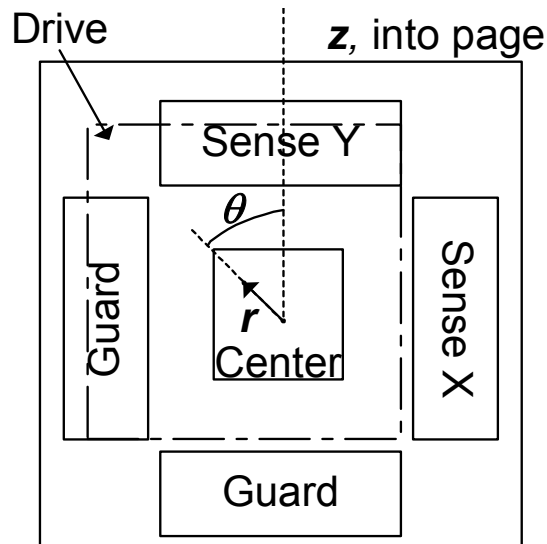


Fig. 4. The *Drive* electrode (dashed box) is shown in one of the simulated positions in relation to the bottom plate with $r=420$ microns and $\theta=45.0^\circ$. In this case, C_Y is larger than C_X .

5. RESULTS

5.1. Uniqueness of a solution

The primary goal of defining a relationship between spatial location (X, Y, Z) and capacitances (C_X, C_Y, C_C), is to show a unique location associated with each set of sensed capacitances. The configuration of the center electrode, S_C was chosen to maintain a near-constant value for a constant plate separation. Fig. 5 only shows the mean of C_C values for a given plate separation, z , since the variation was quite small between all 128 points. Fig. 6 displays segments of the valid values of C_X, C_Y when normalized by C_C and noticeably forms the base of a large cone. For large values of z , the dynamic range and sensitivity of the sensor decreases as C_X and C_Y approach each other in value. Fig. 7 shows the non-normalized plot of C_X and C_Y for a constant z . For a small z , C_X and C_Y have a large dynamic range. For a constant plate separation, there are no points of symmetry where the C_X and C_Y values could be the same. This is due to the fact that the *Drive* electrode never completely overlaps either the S_X or S_Y electrodes in the modeled region.

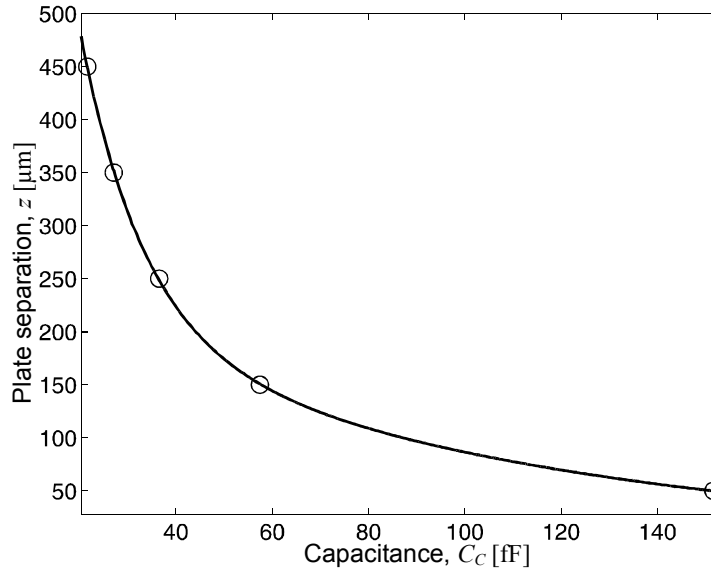


Fig. 5. Capacitance on the *Center* electrode, C_C , depends strongly on plate separation, z . The fitted exponential curve is shown above.

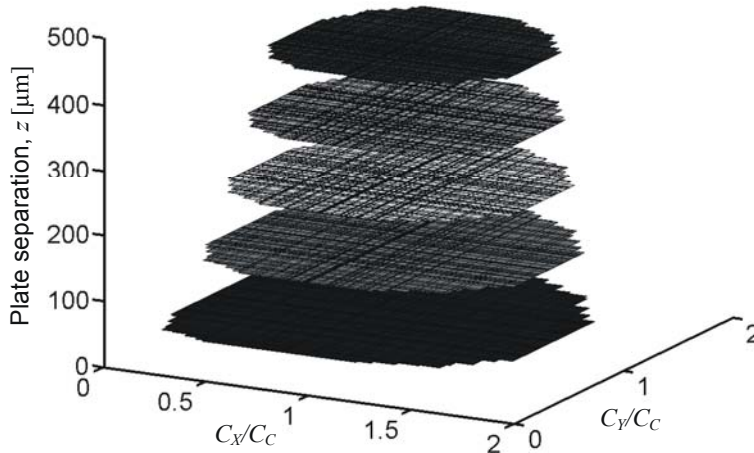


Fig. 6. C_X and C_Y normalized by C_C showing small variation in capacitance ratio.

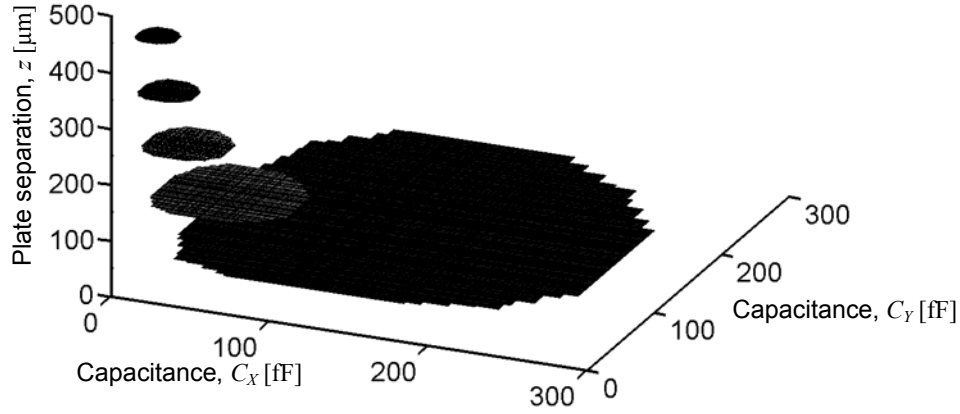


Fig. 7. C_X and C_Y without normalization against plate separation, z . This surface plot shows the large range of possible values of C_X and C_Y for a given plate separation.

5.2. Transfer functions

The theoretical analysis of a capacitive sensor where parallel plate idealities cannot be assumed is a great candidate for an analytical solution where a curve is fit to the data collected. The plate separation is straightforward to calculate due to its direct relationship to C_C . However, the curve fitting of C_X and C_Y required some assumptions to keep the equations simple. Fringing electric fields occur to a small degree and cause a deviation from ideal parallel plate calculations, making the curves deviate from more straightforward equations.

Equation (2) describes a surface for which X is valid. After approximating as a plane, X only depends on C_Y and C_C .

$$X(C_Y, C_C) = -a + \frac{(-b - c * C_Y)}{(d + e * C_C)} \quad (2)$$

where $a = 310$, $b = -1.50 \times 10^8$, $c = 1.43 \times 10^7$, $d = 3.03 \times 10^5$, and $e = -3.70 \times 10^4$. The relationship between C_X , C_Y and X , can be described as a plane with a linear dependence on C_C . Y also depends on C_X and C_Y for the same reason. Equation (3) relates Y to C_X and C_C after a small approximation to set dependence on C_Y to zero displacement. This equation is symmetric to X due to the symmetry on the sensor itself.

$$Y(C_X, C_C) = -a + \frac{(-b - c * C_Y)}{(d + e * C_C)} \quad (3)$$

where $a = 313$, $b = -1.34 \times 10^8$, $c = 1.24 \times 10^7$, $d = 2.72 \times 10^5$, and $e = -3.18 \times 10^4$. Equation (4) relates Z displacement to capacitance and is only a function of C_C . This requires a very small approximation since C_C could slightly depend on lateral displacements instead of only on plate separations if the plates were displaced a larger distance. Large lateral displacements are not within the calculation range and are assumed invalid for this sensor design. The specific use of guard electrodes to ensure a consistent non-fringing electric field around the central sensing electrode, S_C , allowed for this strong dependence.

$$Z(C_C) = a * \exp(b * C_C) + c * \exp(d * C_C) \quad (4)$$

where $a = 1320$, $b = -0.0765$, $c = 246$, and $d = -0.0105$. A unique solution for X , Y and Z is known to exist only for the range simulated, however, these equations will be tested for extensibility into a larger space of solutions in the near term.

6. TEMPERATURE AND HUMIDITY MATERIALS INVESTIGATION

Initial research into highly temperature dependant dielectric materials has so far yielded several materials worth future analysis. The temperature range desired is 0-50° Celsius and one candidate with a large temperature dependence in this range is $Ba_{1-x}Sr_xTiO_3$ ¹⁴. This thick-film material exhibits a relative dielectric permittivity swing from ~2500 to ~10 for the molecular formula with $x=0.5$ ($Ba_{0.5}Sr_{0.5}TiO_3$). Polyimides were found to be a common solution to thin-film humidity sensing applications^{15,16,17}. Kapton and Upilex are commonly known polyimides and will be weighed along with other solutions for the humidity-sensing portion of this sensor.

7. SENSOR FABRICATION METHODS

The sensitive skin cell presented in this paper is designed to be built by standard thin-film manufacturing techniques. The primary core material will be a uniform thickness high-density foam rubber. The electrode patterns on the bottom layer (which includes *Sense X* and *Sense Y*) will be copper patterned onto a flexible plastic material with a solid ground backplane. The top layer electrode pattern will also be created with copper but will have thin film patterns of the temperature and moisture sensitive materials to be determined at a later date. These layers will then all be sandwiched together and combined with thin-film amplifier circuitry.

8. CONCLUSIONS AND FUTURE WORK

The authors have simulated and verified a sensitive skin pixel that has the ability to measure normal and shear forces. Simulations have been completed to demonstrate the capability of detecting temperature and humidity dependant dielectrics using two independent fringed-electric field electrodes on the same sensor cell. One area that needs to be addressed is the density change in the compressible middle layer. This was not considered for this simulation, but future simulations must take into account affects of a variable dielectric middle layer. In the near term, functional materials will be chosen and the microfabrication techniques will be assessed in order to create a flexible prototype sensor. The humidity and temperature are two key items, which could provide enough information to increase the sensitivity and resolution of a dielectrometry sensor. Dielectrometry of the skin and prosthetic device interface could allow measurement of skin temperature and moisture to detect pressure sores beginning to form. The sensor could also be used as a haptic device for tele-surgery where the humidity and temperature information could find unique uses for the situation.

ACKNOWLEDGMENTS

This work is partially supported by the National Science Foundation CAREER Award Grant #0093716 and the Washington NASA Space Grant Scholarship. Authors express thanks to Arpi Shaverdian for her research efforts on temperature and humidity dependent materials.

REFERENCES

1. Guglielmelli, E., Genovese, V., Dario, P., and Morana, G., "Avoiding Obstacles by Using a Proximity US/IR Sensitive Skin", *Proceedings of the 1993 IEEE/RSJ International Conference on Intelligent Robots and Systems*, pp. 2207-2214, 1993.
2. Lumelsky, V. and Cheung, E., "Towards Safe Real Time Robot Teleoperation: Automatic Whole-sensitive Arm Collision Avoidance Frees the Operator for Global Control", *Proceedings of the 1991 IEEE International Conference on Robotics and Automation*, pp. 797-802, 1991.
3. Webster, J. G., *Tactile Sensors for Robotics and Medicine*, John Wiley & Sons, 1988.
4. Lumelsky, V. J., Shur, M. S., and Wagner, S., "Sensitive skin", *IEEE Sensors Journal*, **1**, pp. 41-51, 2001.
5. Chase, T. A. and Luo, R. C., "A Thin-Film Flexible Capacitive Tactile Normal/Shear Force Array Sensor", *IEEE 21st International Conference on Industrial Electronics, Control, and Instrumentation*, **2**, pp. 1196-1201, 1995.
6. Lazzarini, R., Magni, R., and Dario, P., "A Tactile Array Sensor Layered in an Artificial Skin", *Proceedings of the IEEE International Symposium on Industrial Electronics*, pp. 54-59, 1996.

7. Liu, R. H., Wang, L., and Beebe, D. J., "Progress towards a smart skin: fabrication and preliminary testing", *International Conference of the IEEE Engineering in Medicine and Biology Society*, **4**, pp. 1841-1844, 1998.
8. Kane, B. J., Cutkosky, M. R., and Kovacs, G. T. A., "A traction stress sensor array for use in high-resolution robotic tactile imaging", *Journal of Microelectromechanical Systems*, **9**, pp. 425-434, 2000.
9. Kane, B. J., Cutkosky, M. R., and Kovacs, G. T. A., "CMOS-compatible traction stress sensor for use in high-resolution tactile imaging", *Sensors and Actuators A: Physical*, **54**, pp. 511-516, 1996.
10. Jin, W. L. and Mote, C. D., "Development of a six-component miniature force sensor using silicon micromachining and conventional machining technologies", *IEEE Transactions on Instrumentation and Measurements*, **47**, pp. 715-719, 1998.
11. Jin, W. L. and Mote, C. D., "On the calibration of multicomponent microforce sensors", *Journal of Microelectromechanical Systems*, **7**, pp. 156-163, 1998.
12. Zhu, H., Harris, G. F., Wertsch, J. J., Tompkins, W. J., and Webster, J. G., "A microprocessor-based data-acquisition system for measuring plantar pressures from ambulatory subjects", *IEEE Transactions on Biomedical Engineering*, **38**, pp. 710-714, 1991.
13. Crago, P. E., Chizeck, H. J., Neuman, M. R., and Hambrecht, F. T., "Sensors for Use with Functional Neuromuscular Stimulation", *IEEE Transactions on Biomedical Engineering*, **33**, pp. 256-268, 1986.
14. Wenmin, Q., Green, R., and Austin, M., "Development of multi-functional sensors in thick-film and thin-film technology", *Measurement Science and Technology*, pp. 1111-1118, 2000.
15. Denton, D. D., Day, D. R., Priore, D. F., Senturia, S. D., Anolick, E. S., and Scheider, D., "Moisture Diffusion in Polyimide Films in Integrated Circuits", *Journal of Electronic Materials*, **14**, pp. 119-136, 1985.
16. Ralston, R. K., Klein, C. F., Thoma, P. E., and Denton, D. D., "A Model for the Relative Environmental Stability of a Series of Polyimide Capacitance Humidity Sensors", *Sensors and Actuators B: Chemical*, **B34**, pp. 343-348, 1996.
17. Schubert, P. J. and Nevin, J. H., "A Polyimide-Based Capacitive Humidity Sensor", *IEEE Transactions on Electron Devices*, **ED-32**, pp. 1220-1223, 1985.